PROCEEDINGS, 51st Workshop on Geothermal Reservoir Engineering
Stanford University, Stanford, California, February 9-11, 2026
SGP-TR-230

Deconstructing the Crustal Heat Extraction of UtahForge Engineered Geothermal System

Peter Leary[1] & Peter Malin[2]

[1]Geoflow Imaging Ltd 43 High St, Auckland 1010, New Zealand

[2]Earth and Climate Sciences Duke University

peter@geoflowimaging.com; malin@duke.edu

Keywords: EGS, ambient crust, poro-permeability, microseismicity

ABSTRACT

Engineered Geothermal System (EGS) cross-well flow of V ~ 30L/s @ Q ~ 20MWth for 30 days was observed by the UtahForge project in 2024. Stimulation data are deconstructed into four steps : (i) wellbore-centric flow V in/out of ambient crust poro-permeability; (ii) flow stimulation of poro-permeable ambient crust; (iii) heat advection in the cross-well volume; (iv) heat conduction into the cross-well volume. Data constraints are: (i) Q = ρCTV, ρC = fluid heat capacity, T = crustal temperature, V = wellbore flow; (ii) V ~ $2\pi r0\varphi v0\ell$ for bulk fluid flow φv0 for wellbore of radius r0 ~ .1m and length ℓ ~400m; (iii) grain-scale solid-fluid heat transfer for ambient crust poro-permeability κ(x,y,z) ~ exp(αφ(x,y,z)) to give Peclet number Pe ~ r0φv0/D ~ 10 for thermal diffusivity D ~ 10-6 m2/s; (iv) radial heat conduction for central advective line-sink of strength Q/ℓ. Step (iii) is attested by microseismic emissions recorded by downhole sensors. Step (iv) central line-sink analytics gives heat reservoir lifetimes τ ~ 3-10 years for the UtahForge 100m cross-well offset. As the heat depletion scales with heat removal rate Q, the UtahForge data show how upscaling EGS Q requires upscaling cross-well offsets. The association of EGS microseismicity with κ(x,y,z) ~ exp(αφ(x,y,z)) poro-permeability gives observational means to monitor the UtahForge system and to quantify the future of EGS

1, INTRODUCTION

In 2024 the UtahForge Engineered Geothermal System (EGS) project completed a km-long horizontal wellbore doublet with 100m vertical offset in T ~ 185°C tight crystalline rock [1]. The intent was to hydrofracture a series of well-to-well discrete stress-aligned planar-like flow channels through which to pass a working fluid to conductively extract crust heat as per decades-long conceptual planning [2-5]. After some dozen hydrofracture attempts conducted in both wellbores, no envisioned well-to-well planar flow channels were achieved [1]. In a final cross-well pressurization set-up, all hydrofracture interval packer gear was drilled out of both wells to leave an ℓ ~ 400m reach of an essentially open wellbore-pair. When the entire ℓ ~ 400m length of open injection wellbore was pressurised with surface temperature fluid, it was immediately observed that ambient crust temperature T ~ 185°C fluids flowed from the producer well. The rate of cross-well flow was V ~ 30L/s ~ 3 10^{-2} m^3/s The rate of heat energy produced was Q = ρCTV ~ 4MJ/m^3/ °C x 185 °C x 3 10^{-2} m^3/s ~ 20MWth, ρC = water heat capacity. This steady-state flow was observed for 40 days. With these flow data, the UtahForge cross-well stimulated low project achieved the first commercial grade ambient crust EGS result.

The UtahForge result leaves, however, several open questions. First, what was the actual flow stimulation mechanics? Second, how long will the 100m offset cross-well flow system run before cooling of the ambient crust heat store diminishes its utility? Third, how feasible is it to upscale heat production Q by stimulating flow across cross-well offsets > 100m?

We address these questions via a four-step deconstruction of EGS flow stimulation involving fluid-rock interactions in a realistic ambient crust. Fluid flow in the ambient crust is conditioned by the poro-permeability empiric κ(x,y,z) ~ exp(αφ(x,y,z)), where φ(x,y,z) is a volumetric distribution of pink-noise spatial fluctuations at all scales from cm to km, and α is poro-connectivity parameter that controls the degree by which pore-fluids communicate [6-10]. The poro-permeability empiric κ(x,y,z) ~ exp(αφ(x,y,z)) is attested by well-logs, well-core, and well-flow worldwide [6-8.]. The poro-connectivity parameter α is attested across the value range given by 2-3 < $\alpha\underline{\varphi}$ < 5-6 for geological formations of mean porosity 0.003 < $\underline{\varphi}$ < 0.2 [9]. Finally, also widely attested is the intimate relation between ambient crust microseismicity (Meqs) and the poro-permeability empiric κ(x,y,z) ~ exp(αφ(x,y,z)) [10].

On the basis of the physical nature of fluid-rock interaction, the Step (i) deconstruction of the UtahForge EGS flow stimulation system recognises that wellbore fluids injected into the ambient crust flow into an unknown and essentially unknowable distribution of permeability that connects flow at all scale lengths. Accordingly, it is apparent that cross-well flow is a complex disseminated process of activating pre-existing poro-permeability flow structures that can in principle enable flow from anywhere in the injection well to anywhere in the production well. The key feature is that wellbore fluid pipe-like flow ceases at the wellbore radius; nowhere in the crustal medium is fluid flow pipe-like. Deconstruction Step (ii) recognises that fluid flow out of or into a wellbore V ~ $2\pi r_0\varphi v_0\ell$ involves collective bulk

Darcy flow velocity φv_0 at each point along the open wellbore interval . **By** conservation of mass, the collective Darcy velocity scales inversely with distance from the wellbore $v(r) = r_0 v_0 / r$. Collectively, the Darcy flow fluid is in grain-scale contact with the granular heat store whatever the local complexity of poro-permeability structure. In deconstruction Step (iii), the collective fluid flow can increase if the local poro-connectivity α parameter increases via the elevated fluid pressure. To first order, increasing poro-connectivity does not involve increasing porosity and thus to first order does no work against the large confining stresses. We thus have a new energetically favoured means of flow stimulation consistent with both the pre-existing poro-permeability distribution and with heat transport by advection rather than conduction. With the recognition of heat advective transport within the stimulation value, EGS deconstruction Step (iv) addresses the conductive supply of heat from the surrounding crust which will supply heat to the advection process stimulation volume. In this step the UtahForge EGS flow stimulation system is approximated as a single central line-sink of radius R and Q/ℓ radial heat flux boundary condition embedded within a crustal mass of thermal diffusivity $D \sim 10^{-6}$ m^2/s at temperature T. The analytic solution for the thermal mass $T(r,t)$, $r > R$, serves to estimate the thermal history of the UtahForge system at the radius $r_p \sim 50\text{m} > R$, the radial location of the production well.

2. UTAHFORGE EGS STIMULATION PRIJECT DECONSTRUCTION

The UtahForge EGS flow stimulation system geometry is sketched in Fig 1. The sketched crustal volume is defined throughout by poro-permeability $\kappa(x,y,z) \sim \exp(\alpha\varphi(x,y,z))$, with the cross-well sub-volume defined by stimulated poro-connectivity parameter $\alpha_s > \alpha$. The greater poro-connectivity parameter stimulates flowability in the cross-well volume without doing work against the confining stresses. The four following subsections describe the four aspects of the UtahForge EGS flow stimulation system outlined above.

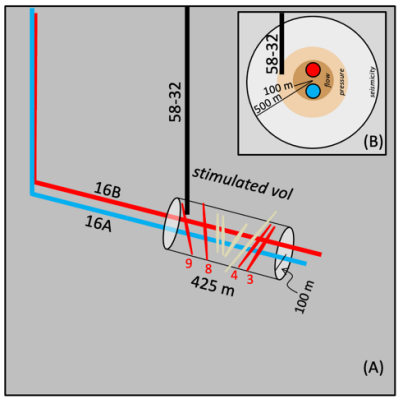

Figure 1. Sketch of UtahForge EGS stimulation flow system geometry [11]. The crustal volume is defined throughout the sketch volume by a poro-permeability distribution $\kappa(x,y,z) \sim \exp(\alpha\varphi(x,y,z))$, with the cross-well crustal volume of 100m diameter having a stimulated poro-permeability $\kappa_s(x,y,z) \sim \exp(\alpha_s \varphi(x,y,z))$, with the poro-connectivity parameter having a stimulated value $\alpha > \alpha$, increasing cross-well flow without increasing cross-well porosity. .

2.1. FLUID IN/OUT FLOW FOR THE WELLBORE PAIR -- Q = PCTV

EGS flow system heat energy production is the product of fluid volumetric heat capacity ρC, crustal temperature T, and wellbore fluid volumetric flow V, $Q = \rho CTV$. For water heat capacity $\rho C \sim 4.2\text{MJ/m}^3/^o\text{C}$, crustal temperature at $T \sim 185^o\text{C}$ and production wellbore volumetric flow $V \sim 30\text{L/s} \sim 3\ 10^{-2}\text{m}^3/\text{s}$, the UtahForge EGS flow system produces $Q \sim 23\text{MW}$ of heat energy flow. For a commercial perspective , direct-use energy applications at 1.5 cents per kWh, the UtahForge EGS system returns ~ $3M heat energy equivalent per annum. The utility of $Q \sim 23\text{MW}$ heat energy rate depends on how long the rate can be maintained. We can also note further that $Q \sim 20\text{NW}_{th} \sim 2\text{MW}_e$ is at the lowest end of commercial power electrical generation spectrum ranging from 2MW_e to 20MW_e with the majority between 3MW_e and 10MW_e [12], thus prompting the question of how feasible it will be to scale up the UtahForge EGS stimulation process.

2.2. WELLBORE COUPLING TO AMBIENT CRUST PORO-PERMEABILITY EMPIRIC K(X,Y,Z) ~ EXP(AΦ(X,Y,Z))

With reference to Fig 1, the UtahForge EGS flow stimulation plan was to site a series of isolated hydrofracture along the ℓ ~ 400m horizontalwell-pair reach [1]. As per the long-standing stimulation expectation [2-5], well-to-well flow stimulation would occur via discrete stress-aligned planar-like cubic-law flow channels through which to pass a working fluid to conductively extract crust heat as per decades-long conceptual planning. In the event, after some dozen hydrofracture attempts conducted in both wellbores, no envisioned well-to-well planar flow channels were achieved [1]. In a final cross-well pressurisation set-up, all hydrofracture interval packer gear was drilled out of both wells to leave an ℓ ~ 400m reach of an essentially open wellbore-pair. As seen in Fig 2,as soon as the injection well pressurisation began at 50 minutes (blue trace pressure at left, red trace flow rate right), the open wellbore pair immediately passes well-to-well fluid fluid (blue flow rate trace at right). With passing time the injector pressure grows and the injector and producr flow rates grow in lock step. Whn at 300 minutes the inpector pressure is interrupted, the injector and producer flow rates drop . The is a clear well-to-well flow connectivity between the open injector well and the open producer well that did not exist when hydrofrack fluids were injected at either the injector or producer wells [1]. Well-to-well flow connetivity is logically inferred to be distributed over the entire the ℓ ~ 400m horizontal well-pair reach as per the ambient crust empiric κ(x,y,z) ~ exp(αφ(x,y,z)).

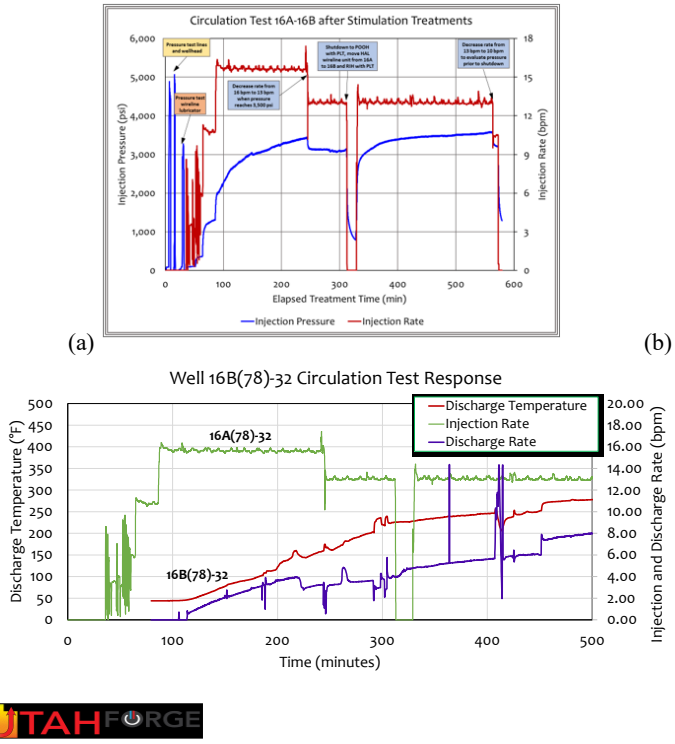

Figure 2. UtahForge EGS stimulation flow data Figs 25 and 26 from 2024 stimulation treatment report [1]. (a) Injector wellbore pressurisation of 400m length of open hole (blue trace) > 0 at ~ 50 minutes. (b) Fluid flow rates in injector (red) and producer (blue) wellbores beginning at the time of injector pressurisation. The producer well flow rate lags the injector flow rate due to finite fluid flow travel time over the 100m well-pair separation. Well-to-well flow occurs immediately with pressurisation, indicating that the EGS stimulation procedures created well-to-well flow connectivity within the cross-well volume that was accessible to the whole-well pressurisation fluid column that were not available to the discrete isolated hydrofrack intervals. We can conclude that well-to-well flow occurs via the disseminated volumetric poro-permeability distribution κ(x,y,z) ~ exp(αφ(x,y,z))accessed by the 400 meters of open hole pressurisation fluids. .

During the pressurisation of the 400m length of open injector well shown in Fig 2, a pressure/flow logging tool in the injector well measured the wellbore fluid flow along the length of the pressurisation interval. Fig 3 shows that the wellbore flow along the 400m pressurisation interval was more less uniform. This is direct evidence that the injector fluid was exiting the open wellbore at rates

consistent with exit flow averaged over extended wellbore lengths of poro-permeability $\kappa(x,y,z) \sim \exp(\alpha\varphi(x,y,z))$ rather than exit flow confined to narrow hydrofrack intervals.

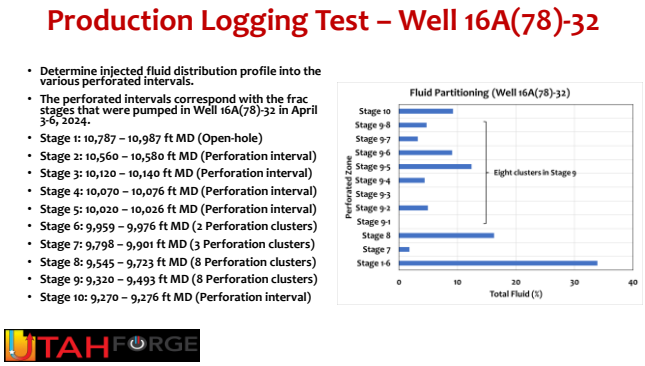

Figure 3. UtahForge EGS stimulation flow data Fig 27 from 2024 stimulation treatment report [1]. Injector flow data showing that during the Fig 2 pressurisation of the entire length of the injector well, injector wellbore fluid exited the well nearly uniformly along the 400m open well reach. The exiting fluid was not constrained to limited wellbore intervals by packers used in the earlier sequence of cross-well hydrofrack attempts, evidence that open wellbore intervals access the full range of ambient crust poro-permeability flow paths given by $\kappa(x,y,z) \sim \exp(\alpha\varphi(x,y,z))$. .

It is evident from the Figs 2-3 primary UtahForge EGS stimulation well-to-well flow data that cross-well flow occurs volumetrically rather than being confined to the envisioned discrete pipe-like planar cross-well flow paths. The inferred Fig 1 volumetric flow distribution nature is further attested by ancillary microseismic emissions throughout the greater UtahForge stimulation volume. As discussed below, EGS microseismicity event size and spatial-correlation spatial distributions indicate that EGS injected fluids pass into the surrounding crust via the poro-permeability distribution $\kappa(x,y,z) \sim \exp(\alpha\varphi(x,y,z))$ attested by well-log, well-core, and well-flow data worldwide [6-10].

The UtahForge EGS production well volumetric flow is related to the crustal cross-well flow as $V \sim 2\pi r_0 \varphi v_0 \ell$, where φv_0 is bulk fluid flow into an open wellbore interval of radius r_0 and length ℓ. Bulk flow denotes Darcy fluid velocity v_0 in a medium of porosity φ, and well-to-well flow is taken to have effective angular aperture of 2π. By conservation of mass, $v(r) = v_0 r_0/r$ at radial offsets $r > r_0$ at least near the wellbore, giving $V \sim 2\pi r_0 \varphi v_0 \ell$ in terms of mean values of porosity and fluid velocity averaged along the open wellbore length $\ell \sim 400$m and the 100m wellbore-pair offset. The deconstruction thus features Darcy flow v(r) denoting heat advection rather than heat conduction as the primary heat transfer process of EGS systems in the ambient crust.

At this point it becomes logical to gauge the role of advection in the UtahForge EGS system via the Peclet number $Pe = r_0 \varphi v_0/D$, for thermal diffusive $D \sim 10^{-6}$ m^2/s. For $r_0 \varphi v_0 \sim V/2\pi\ell \sim 10^{-5}$ the Peclet number for the UtahForge EGS system is $Pe \sim 10$. For purposes of comparison with the long-standing concept of EGS via conduction processes [2-5], the present advection system is 10 times more heat energy productive than any heat extraction system bound by thermal conduction which is functionally equivalent to $Pe \sim 1$. In addition to marking the contrast to decades of EGS process concepts firmly tied to conduction processes, $Pe \sim 10$ ties the EGS flow system to other wellbore-temperature data clearly related to crustal flow in fractures. Peclet values $5 < Pe < 10$ are observed for isolated wellbore interval in two wellbore-temperature data sets from naturally occurring deep crustal wellbores [13-14]. We are logically entitled to infer that UtahForge EGS flow stimulation has boosted incidental natural fracture advective flow in range $5 < Pe < 10$ to $Pe \sim 10$ for the extended decameters-long stimulation interval at the UtahForge site. .

2.3. CROSS-WELL FLOW STIMULATION OF REALISTIC PORO-PERMEABILITY CRUST -- $K(X,Y,Z) \sim EXP(A\Phi(X,Y,Z)) \rightarrow K_S(X,Y,Z) \sim EXP(A_S \Phi(X,Y,Z))$

The stimulation mechanics by which UtahForge wellbore treatments enhance the cross-well flow documented in Figs 2-3 are logically due to alterations in the local cross-well poro-permeability field $\kappa(x,y,z) \sim \exp(\alpha\varphi(x,y,z))$. Again, logically, the changes are those

involving the least expenditure of deformation energy. It is thus logical that porosity changes are minimal because increasing porosity necessarily works against the large confining stresses. Far less energy is required to change the poro-connectivity parameter $\alpha \rightarrow \alpha_s > \alpha$. Fig 4 illustrates the degree to which the poro-connectivity parameter α naturally occurs in a suite of reservoir formations [9]. Each subplot shows how well-core log(permeability) scales with well-core porosity across a crustal formation, $\delta\log(\kappa) \sim \alpha\delta\varphi$. The observed physical relation duplicates the well-known Stirling formula combinatorial relation $\delta\log(N!) \sim \alpha\delta N$, where N is the number of pores in a unit volume and N! is the number of connections possible for the N pores within the unit volume. With many physical factors in play deterring each formation α value, it is clear that α can have a range of values, and logical that UtahForge stimulation treatment can alter α values without significantly altering porosity. Fig 5 illustrates in two dimensions how changing the poro-connectivity value can change the bulk fluid flow velocity without expending energy changing porosity. The implied stimulation mechanics stands in marked contrast to the decades-long supposition of creating planar-gap flow channels that necessarily requires expending energy doing work against crustal confining pressures.

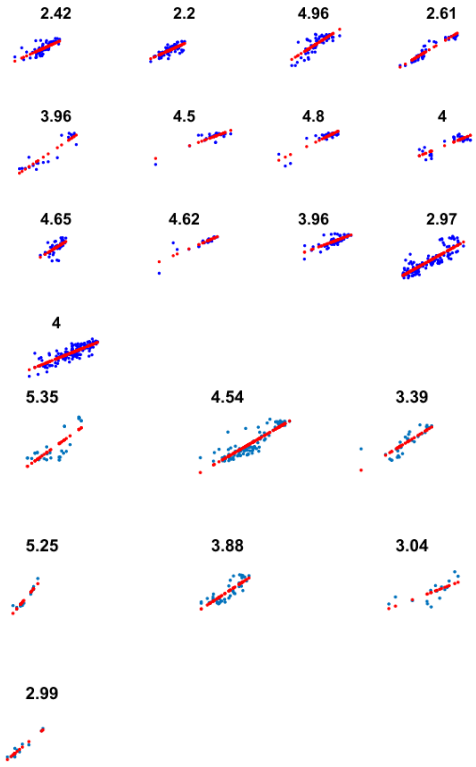

Figure 4. Plots of porosity (horizontal axis) against log(permeability) (vertical axis) for sequences of reservoir formations in South Australia [9]. The slope of each plot gives the value of poro-connectivity α for each formation. The range of naturally occurring α values indicates the plausibility that UtahForge cross-well pressurisation treatments can alter α within the cross-well volume. .

The relation of the poro-connectivity parameter α and flow stimulation mechanics is illustrated in Fig 5 [8]. A cross-well pressure field drives wellbore fluids across a crustal section of poro-permeability $\kappa(x,y,z) \sim \exp(\alpha\varphi(x,y,z))$. Darcy fluid flow velocity for low α (a) shows little spatial variation on the scale of the cross-well gap. The flow velocity distribution is dramatically different for large α (b), where pronounced poro-connectivity structure appear at all scales. From Fig 4 we see that poro-connectivity parameter α naturally varies in the ambient crust. EGS stimulation concentrates the otherwise natural poro-permeability variations into a local zone of high pore-cluster-to-pore-cluster flow. We note here that the increased poro-connectivity formally involves no change in porosity. While it is unlikely that no porosity changes occur in physical EGS stimulation processes, the amount of deformation energy expended in increasing α is small compared with systematically creating planar flow-structure gaps as per the traditional stimulation concept [2-5].

Equally importantly, we see in Fig 5 a strong a priori case for EGS stimulation processes to create a vast range of microseismic emissions activity in the cross-well volume. A signal feature of ambient crust microseismicity is a close connection between the spatial statistics of the poro-permeability and the spatial statistics of the microseismicity [8]. This relation is developed in Section 3 below.

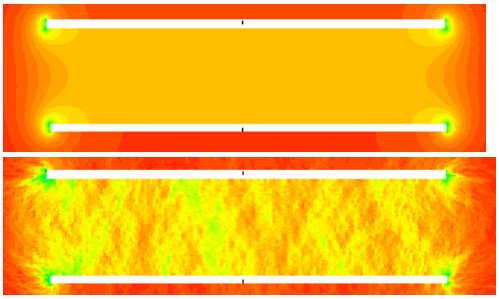

(b)

Figure 5. Cross-well Darcy fluid flow for poro-permeability media distributions κ(x,y,z) ~ exp(αφ(x,y,z)) with low α (a) and high α (b). An important feature of the illustrated EGS crustal stimulation process is that the concurrent microseismic emissions recorded by local seismic sensors can locate the emission sources in time and space to provide an ongoing image of the stimulation volume. .

2.4. CONDUCTIVE HEAT TRANSPORT INTO THE CROSS-WELL HEAT EXCHANGE

The above deconstruction of the UtahForge EGS stimulation flow system data places heat advection transport comfortably in a natural physical framework characterised by increased poro-connectivity parameter α leading to increased fluid flow velocity and hence increased Peclet number Pe ~ v(r)r/D ~ 12, $r_0 < r < \sim 50$m. We now connect the internal wellbore-to-wellbore heat advection flow system sketched in Fig 1 with its larger external heat volume that conductively feeds heat energy to the internal advection system. This is simply approximated by notionally reconfiguring the internal heat transport from well-to-well flow within an R ~ 50m cylinder that encloses the UtahForge well pair. For a production well at the notional r ~ 50m radius, the well retains ambient temperature fluid. We can thus estimate the lifetime τ of the UtahForge heat store by solving the heat conduction equation radial heat inflow as a notional central well removes heat at rate $Q/\ell \sim \rho CTV/\ell \sim \rho CT/K\ 2\pi K\ r_0\varphi v_0 \sim 2\pi KT\ r_0\varphi v_0/D \sim 2\pi KT$ Pe W/m. By this notional radial flow and heat flux boundary, we reserve both the wellbore-based cylindrical heat flow geometry and the internal advection heat transfer of the UtahForge EGS stimulation advection flow system.

The wellbore-centric time-evolving crustal temperature field is provided by Carslaw & Jaeger [15; §13.5 Eq(17)]:

$$T(r,t) \sim Q\sum_k(1 - \exp(-Dk^2t))/k^2\ (J_0(kr)Y_1(ka) - Y_0(kr)J_1(ka))/(J_1(ka)^2+Y_1(ka)^2), \quad (1)$$

where k is spatial frequency, *a* is the central wellbore radius, r > *a*, ad J_0, J_1, Y_0 , and Y_1 are Bessel functions of first and second kind and first and second order. Fig 6 (a) shows the generic/normalised form of (1) for small values of central wellbore radius a in a crustal volume of r = 100m radius for a period of 30 years. Yellow represents the far-field ambient crustal temperature away from the small central line-sink radius, and blue represents the temperature of the exiting central wellbore fluid as defined by the heat flux boundary condition. Fig 6 (b-d) shows top-down views of temperature distributions for central wellbore radii *a* = 20m, 30m, and 40m. We are interested in the region r ~ 50m showing the crustal temperature at the radius corresponding to the position of the UtahForge production well. For large radii equivalences for the actual well-to-well heat extraction, heat at r ~ 50m is seen to decline from ambient temperature due to heat withdrawal outstripping conductive heat renewal. The Fig 6 (b-d) plots show that the larger the heat withdrawal line-sink radius, the greater the temperature decline at the production position. To more quantitatively measure the temperature decline illustrated in Fig 6, we numerically simulate the heat withdrawal process for a T = 185°C ambient crust as seen in Fig 7.

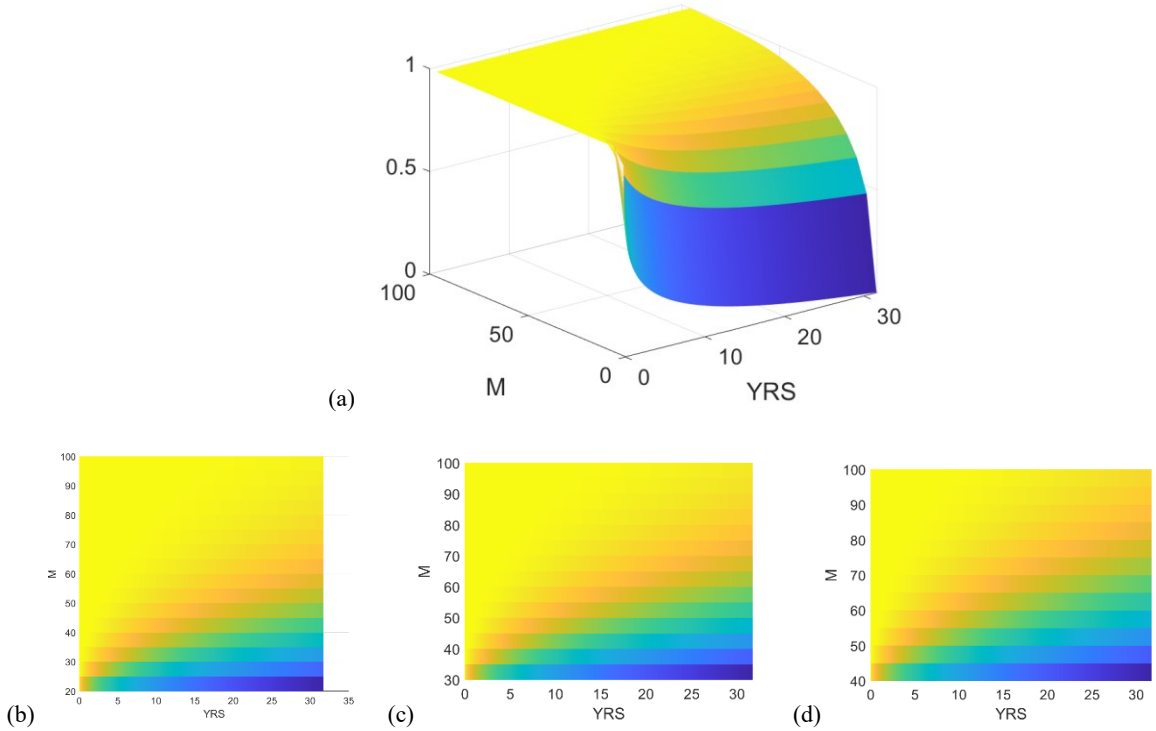

Figure 6. (a) Eq (1) time-evolving radial temperature field $0 < T(r,t) < 1$ for a Fig 1 crustal cylindrical section of radius 150m with a central line-sink of radius a = 10m. Yellow denotes the crustal ambient temperature; blue denotes the line-sink wellbore temperature fixed by the heat flux boundary condition (b-d) Top-down temperature view for heat-sink radii r = 20m, 30m, 40m.

.

Fig 7 (a-c) numerical simulations fix the near-field heat flux boundary condition Q/ℓ at the internal line-sink radii and the external far-field ambient crust temperature at radius r = 150m. The top-down temperature fields are shown for three internal line-sink radii, r = 5m, 15m, and 25m. Our interest is shown by (d), where blue, red, and gold traces profile the time-evolving temperature at the r = 50m radial location of the production well. We see that the r = 5m radius link-sink has little effect on the production well temperature for up to 30 years of production. By contrast, the r = 25m radius line-sink has a significant effect on the production well temperature. For simplicity, the heat flux boundary value is the same for the three internal line-sink radii. Accordingly, the spread of simulated production well temperatures is wider than if the heat flux boundary were adjusted to the same net heat sink extraction rate. In light of the very approximate nature of our computation, allowing the wider production well temperature spread provides a safer illustration of the UtahForge crustal heat store cooling for a Q ~ 20MW, Pe ~10, production well heat energy delivery rate.

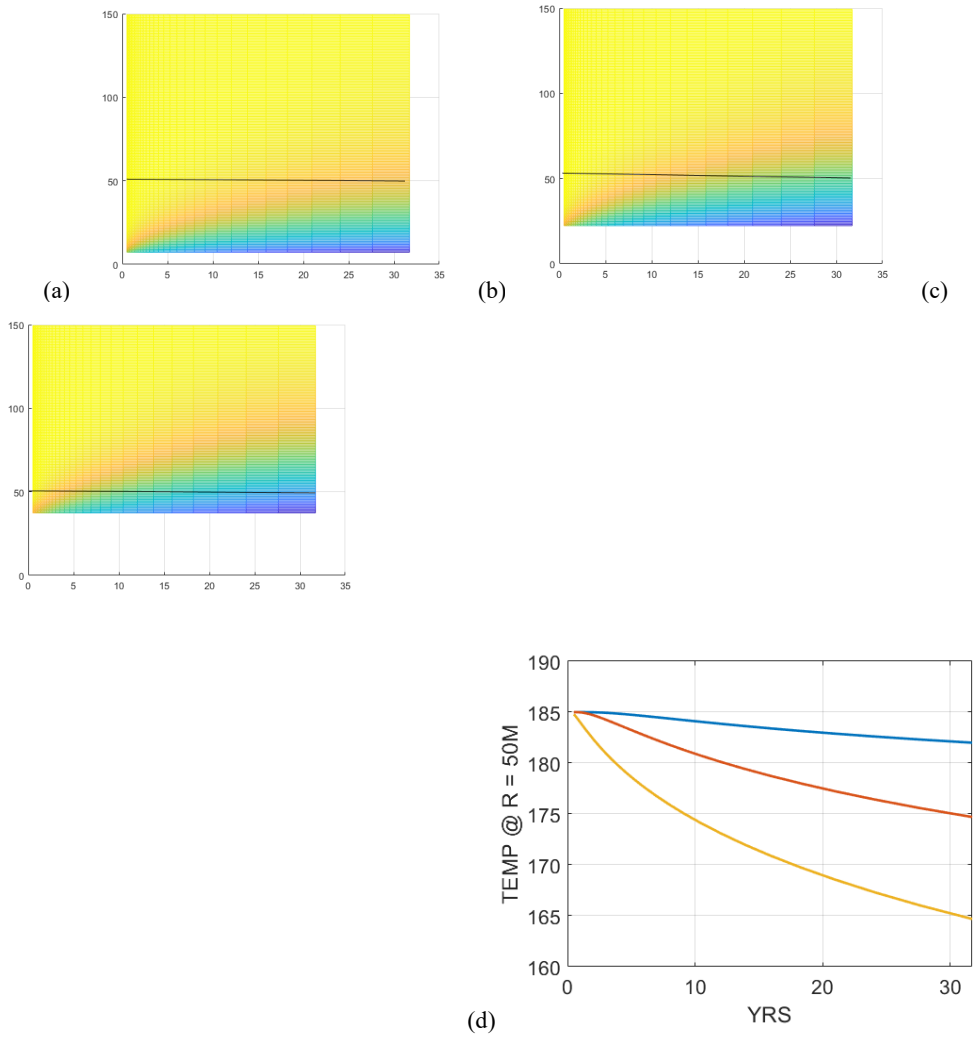

Figure 7. (a-c) Three top-down views of numerical simulations of Eq (1) heat extraction geometry approximation to UtahForge EGS stimulation flow system for heat extraction rate Q/ℓ ~ 20/400MW/m for line-sink radii r ~ 5m, 15m, 25m respectively. Black line represents the UtahForge production well at 50m offset from the central line-sink. (d) Time-evolving temperature profiles for trio of temperature fields at r = 50m radial offset from the line-sink representing the crust temperature at the UtahForge production well. Blue/red/gold traces equate to (a-c) temperature fields. An effective r = 5m line-sink does not affect the production well temperature, while an r = 25m line-sink radius cools the production well temperature by 20°C over 30yrs. A working assumption is that the actual effective line-sink radius lies between these two extremes whereby the production well cools by 10°C after 30 yrs.

Over the spread of Fig 7 heat extraction scenarios, the simulations indicate, first, the viability of a decades-long heat delivery for the present UtahForge EGS stimulation system, while, second, raising questions about the feasibility of achieving significantly higher heat production rates Q >> 20MW, Pe >> 10. Clearly, refining our direct observational knowledge-base for the UtahForge system is called for.

3. UTAHFORGE MICROSEISMIC EMISSION SUPPORT FOR THE EGS DECONSTRUCTION

As given by Eq (1), the UtahForge production well temperature fields scale with heat extraction rate $Q/\ell \sim 2\pi KT$ Pe W/m. Recalling that from $V \sim 2\pi r_0 \varphi v_0 \ell$ and $\ell \sim 400$m, we have $r_0 \varphi v_0 \sim 3\ 10^{-2}$ m^3/s /2π/400m ~ $2.4\ 10^{-5}$ m^2/s to get Pe = $r_0 \varphi v_0/D \sim 12$. For the present UtahForge EGS stimulation flow system, increasing Q/ℓ means increasing Pe through increasing Darcy flow v_0. Further, from Fig 6 we see that

increasing Q/ℓ also means increasing the well-to-well offset as sketched in Fig 2. Two questions arise here: Can we increase v_0, and can we increase the well-to-well stimulation offset?

Prompted by Fig 5 answers to both questions almost certainly lie in what we can learn about EGS from the present UtahForge EGS stimulation structure, and with equal certainty the key to these learnings lies in the EGS stimulation microseismic Meq activity recorded by local downhole seismic sensor strings indicated by the vertical black lines in Fig 1,

EGS crustal flow stimulation is automatically accompanied by microseismic emissions as the injected high-pressure wellbore fluids are forced into the ambient crust. The long-held belief isthat the ambient crust is effectively a quasi-uniform poro-elastic continuum at all relevant scales. In accordance with this belief, it has long been supposed that injected high-pressure fluids will hydrofrack the ambient crust along stress-aligned planes of weakness, and that associated microseismic emissions arise from stress-aligned planar slip surfaces resembling fault-zone-like slip mechanics [16]. With Figs 8-12 we see that a large body of UtahForge EGSS flow stimulation Meq events emphatically negate these fault-like Meq slip mechanics. Instead, Meq slip processes show evidence of being embedded in the ambient crust poro-permeability distribution $\kappa(x,y,z) \sim \exp(\alpha\varphi(x,y,z))$. First, UtahForge Meq events are lognormally distributed in size. Second, the Meqs are pairwise spatially correlated as $G(r) \sim 1/r$ for pair-offset r. Third, Meq first motions are bidirectional rather than unidirectional. We can here note how accurate location of EGS stimulation Meq motions recorded by local downhole sensors allow us to explore the EGS stimulation process in space and time.

Fig 8 illustrates the spatial relation of overall UtahForge EGS stimulation Meqs in relation to the injection/production well-pair [1]. Here the Fig 1 stimulation domain is notionally indicated by the small rectangular patches at the center of the Meq distribution. It is apparent that stimulation fluids extend into the ambient crust far beyond the cross-well volume sketched in Fig 1. In the standard view of EGS, Meq excitation at the large-scale Fig 8 tracks an elongate stress-aligned plane of weakness. While stress effects may indeed influence the Meq distribution, they do not explain the lognormal Meq size distribution, the Meq-pairwise distribution, or the bidirectional rather than unidirectional slip mechanics of Figs 9-11. Rather, these properties emerge naturally from the interaction of stimulation fluids with the ambient crust poro-permeability empiric $\kappa(x,y,z) \sim \exp(\alpha\varphi(x,y,z))$

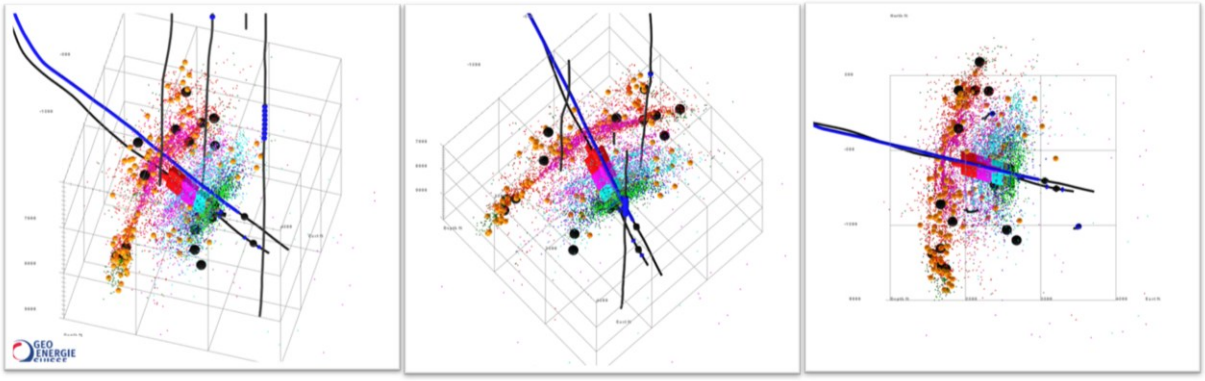

Figure 8. UtahForge EGS stimulation flow structure microseismicity event (Meq) distribution surounding the injection/production well-pair [1]. Rectangles mark the notional position of cross-well stimulation events sketched in Fig 1 Blue dots along vertical sensor wellbores in black denote seismic sensors recording Meq emissions. Figs 9-11 illustrate the internal statistical and dislocation-slip properties of such Meq events that testify to the $\kappa(x,y,z) \sim \exp(\alpha\varphi(x,y,z))$ origin of these EGS-induced seismic emissions. .

The widely distributed Fig 9a UtahForge Meq events recorded in 2022 anticipate the widely distributed 2024 Meq data of Fig 8 [1]. We can see in the Fig 9 data two of the three diagnostic features that characterise ambient crust microseismicity. Fig 9b exhibits the lognormal distribution of Meq events, and Fig 9c exhibits the two-point event-pair spatial correlation distribution function $G(r) \sim 1/r$, r = Meq event-part separation. These observed properties refute the standard view of EGS Meqs: (i) Gutenberg-Richter power-law frequency distribution $N \sim 10^{1-bm}$, m = event magnitude, predicts small event number increase indefinitely (but are not seen in the data), and (ii) Meq locations have no structure (but instead are seen to have spatial correlation $G(r) \sim 1/r$).

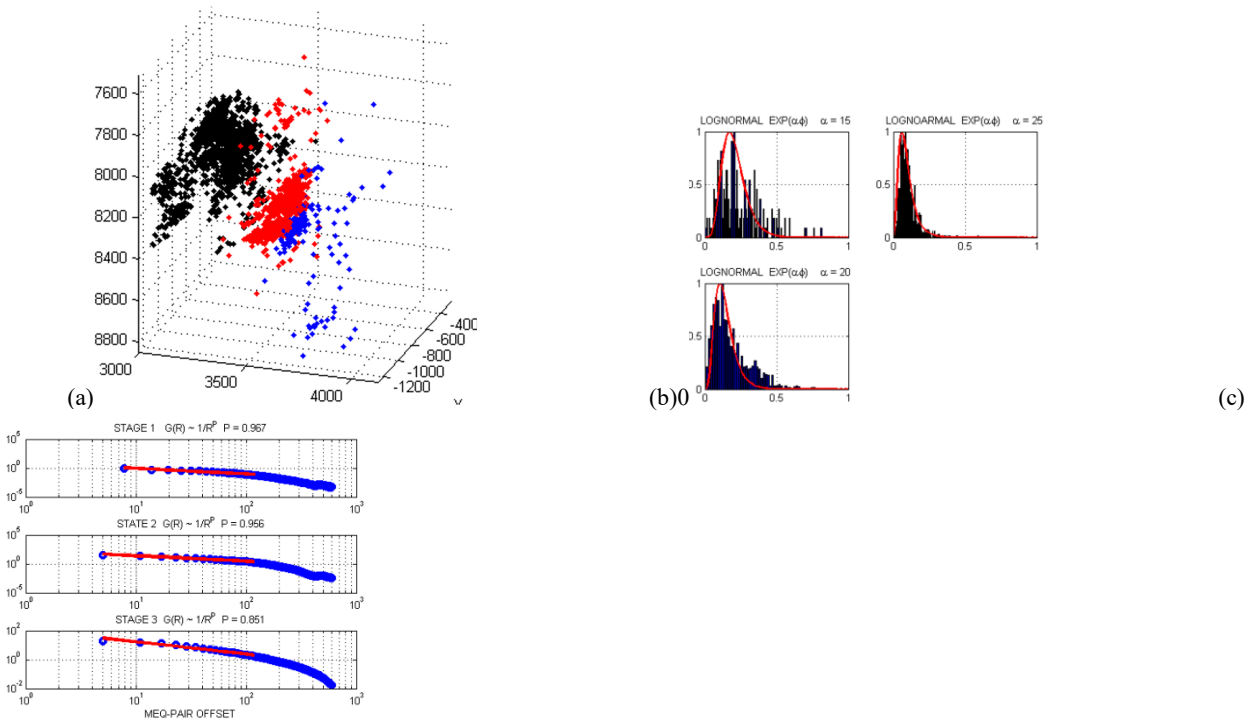

Figure 9. UtahForge EGS stimulation microseismicity (Meq) size and pairwise spatial correlation statistics. (a) UtahForge Meq event location for three stimulations in 2022. (b) Meq moments are lognormally distributed, with small numbers of small moments occurring naturally instead of increasing indefinitely as per the Gutenberg-Richter relation for fault-zone seismicity. (c) Two-point spatial correlation distributions G(r) ~ 1/r, r = pairwise Meq event offsets; in the staandard view Meqs are not correlated. .

Equally important to the Fig 9 negation of standard Meq assumptions are the Fig 10 positive assertions that EGS Meq size and spatial correlation property distributions are congruent with the ambient crust poro-permeability size and spatial correlation distributions given $\kappa(x,y,z) \sim \exp(\alpha\varphi(x,y,z))$. Figs 10a-b display two poro-permeability distributions $\kappa(x,y,z) \sim \exp(\alpha\varphi(x,y,z))$, with (a) having a finite value $2 < \alpha < 4$ as per Fig 4 and (b) having $0.2 < \alpha < 0.4$. Figs 10c-d show the corresponding lognormal versus normal size distributions, and corresponding two-point spatial correlation functions $G(r) \sim 1/r^1$ and $G(r) \sim 1/r^0$. .

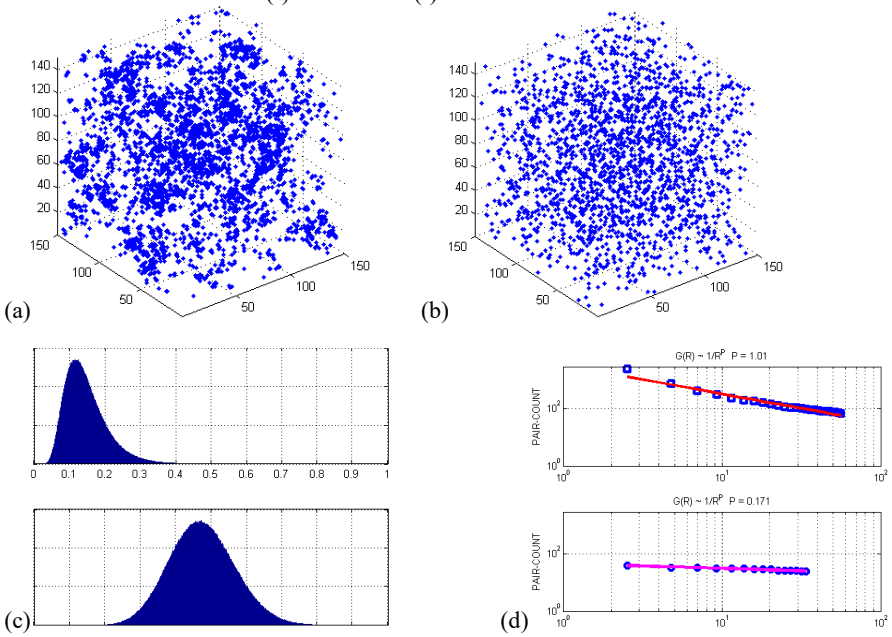

Figure 10. Comparison of two synthetic representations of UtahForge EGS stimulation Meq size and spatial correlation distributions. (a) Meq ev ents occur as dislocation slip within high poro-permeability structures in an ambient crust poro-permeability empiric $\kappa(x,y,z) \sim \exp(\alpha\varphi(x,y,z))$. (b) Meqs are white noise randomly spaced as regularly assumed in discrete fracture network (DFN) constructions. (c) Above is lognormal size distribution of upper left Meqs, below is normal distribution of upper-right random Meqs. (d) Above is the G(r) ~1/r two-point spatial correlation function G(r) ~ 1/r and below is the white noise random spatial correlation function G(r) ~ const. The empiric $\kappa(x,y,z) \sim \exp(\alpha\varphi(x,y,z))$ synthetic Meq size and spatial correlation statistics are identical to those of the Fig 10 UtahForge EGS stimulation Meqs, thus v\validating the working hypotheses that UtahForge EGS stimulations proceed via interacting with the pre-existing ambient crust poro-permeability field.

.

Fig 11 illustrates the seismic first motion property of EGS Meq events that negates standard Meq assumptions [17]. The standard fault-zone dislocation source slip sketched above has a far-field displacement wave motion denoting slip in one direction only, with slip releasing stress from high to low values along the fault. The observed first displacement motion of EGS Meqs is instead bidirectional, with slip in one direction being followed at a later time by slip in the opposite direction. The observed bidirectional slip is logically due to radial expulsion of high-pressure fluids forced into poro-permeability strutures by EGS pressurisation followed by radial pressure release. In radial pressure release, fluid-ejection motion pointing to a far-field sensor arrives earlier than the corresponding radial motion away from the sensor.

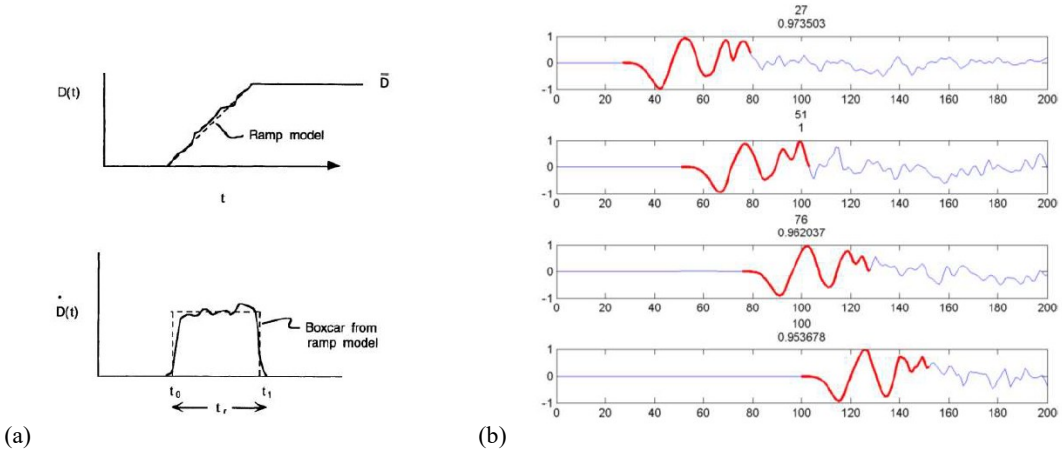

(a) (b)

Figure 11. (a) Unidirectional fault-zone slip-mechanics constant velocity rupture dislocation profile (above) and resultant unidirectional far-field displacement waveform of duration t (below). (b) Bidirectional first motion P-wave displacement waveforms in red recorded at 2kHz sample rate on vertical array sensors in crystalline basement at 2.5km depth directly above a km-scale EGS controlled-stimulation volume at 6km depth.

The EGS stimulation Meq mechanics illustrated in Figs 9-11 establish that injected wellbore fluids migrate through the ambient crust poro-permeability field $\kappa(x,y,z) \sim \exp(\alpha\varphi(x,y,z))$ and over-pressure high permeability structures which then suffer bidirectional dislocation slip in releasing the over-pressuring fluids. In tracing the observed UtahForge EGS stimulation Meq emission process to the $\kappa(x,y,z) \sim \exp(\alpha\varphi(x,y,z))$ poro-permeability field, we establish the systematic means for surveying the stimulation process. As an application of seismic emission tomography, precise Meq waveform timing of seismic motion recorded by the downhole sensor strings seen in Fig 8 allows each event to be precisely located in time and space within the stimulation volume. This Meq survey capability can be used in future stimulation exercises to thoroughly explore the flow structure of the present UtahForge stimulation volume and any future stimulation volumes in the ambient crust.

4. UTAHFORGE EGS STIMULATION MEQ MONITORING AND DEVELOPMENT

Fig 2 cross-well crustal fluid flow in the 2024 UtahForge EGS stimulation volume sketched in Fig 1 opens the door to understanding EGS process at decameter scales at 2.5km depth in the actual ambient crust. As all previous attempts at realizing an EGS procedure for accessing crustal heat at drillable depths have been based on a hypothetical crust assumed to be effectively structureless at all relevant

scales, it is timely that the UtahForge project achieved a result that exhibits the actual crustal properties controlling fluid-rock interactions. Heretofore, any EGS process that was presumed to work at an exploration scale was automatically presumed to work at larger commercial scales. Figs 2-3 EGS flow data are consistent with an ambient crust that is randomly structured at all scales as per the empirical poro-permeability distribution field $\kappa(x,y,z) \sim \exp(\alpha\varphi(x,y,z))$ attested worldwide by well-log, well-core, and well-flow data across the cm-km scale range [6-10]. The pink-noise structured ambient crust poro-permeability undercuts the assumed easy scalability of EGS in the hypothetical structureless crust. Instead, wellbore injected EGS fluids are seen in Figs 8-11 to interact with the poro-permeability $\kappa(x,y,z) \sim \exp(\alpha\varphi(x,y,z))$ that varies unpredictably at all scales. As such, there is a high probability that any EGS fluid injection path meanders according to the pre-existing structured random poro-permeability noise rather than cleaving through a structureless poro-permeability controlled by local stress alignments as assumed in [16].

In compensation for the scaling pink noise complexities of the actual ambient crust flow structures, the UtahForge EGS cross-well stimulation flow data connecting Meq seismic emissions to spatially erratic crustal flow allow observers to remotely explore the physical details of EGS mechanics. Referring to Fig 8, we see that near the EGS stimulation wells there are three vertical wells housing seismic sensor strings. These local seismic sensors record countless Meq seismic emission first motion wavelets traveling in an essentiality uniform seismic wave speed of known logged value. In these circumstances, accurately locating the flow-specific seismic emission source locations is a straightforward exercise in acoustic emission tomography [18-19].

Fig 12 overviews the Meq location inversion process via a numerical simulation of a Fig-8-scale crustal volume of $\kappa(x,y,z) \sim \exp(\alpha\varphi(x,y,z))$ poro-permeability distribution. Fig 12a illustrates porosity-driven wave speed fluctuations in a 2D crustal section followed by the Fig 12b schema of wellbore sensors in the stimulation volume able to record waves emanating from a notional source point asterisk. Fig 12c shows successive source-sensor travel-time data as circles tracked by travel-time curves fit to data by a least-squares Nelder-Mead fitting algorithm. The Nelder-Mead algorithm returns the spatial location of the source point from the collective sensor travel-time arrival data. Fig 12d-e are two views of the fidelity of the inverted source locations (red) in relation to the actual locations (blue) for 30 Meq event locations. These source locations are selected as the 30 largest-value poro-permeability sites in the simulation data cube, and as such conform to the Fig 10a poro-permeability distribution. The spatial resolution of the inversions is shown respectively at decameter - and meter-scales. Such an Meq data acquisition and processing conducted at the UtahForge EGS stimulation site can routinely confirm in detail the nature and progress of the EGS stimulation process.

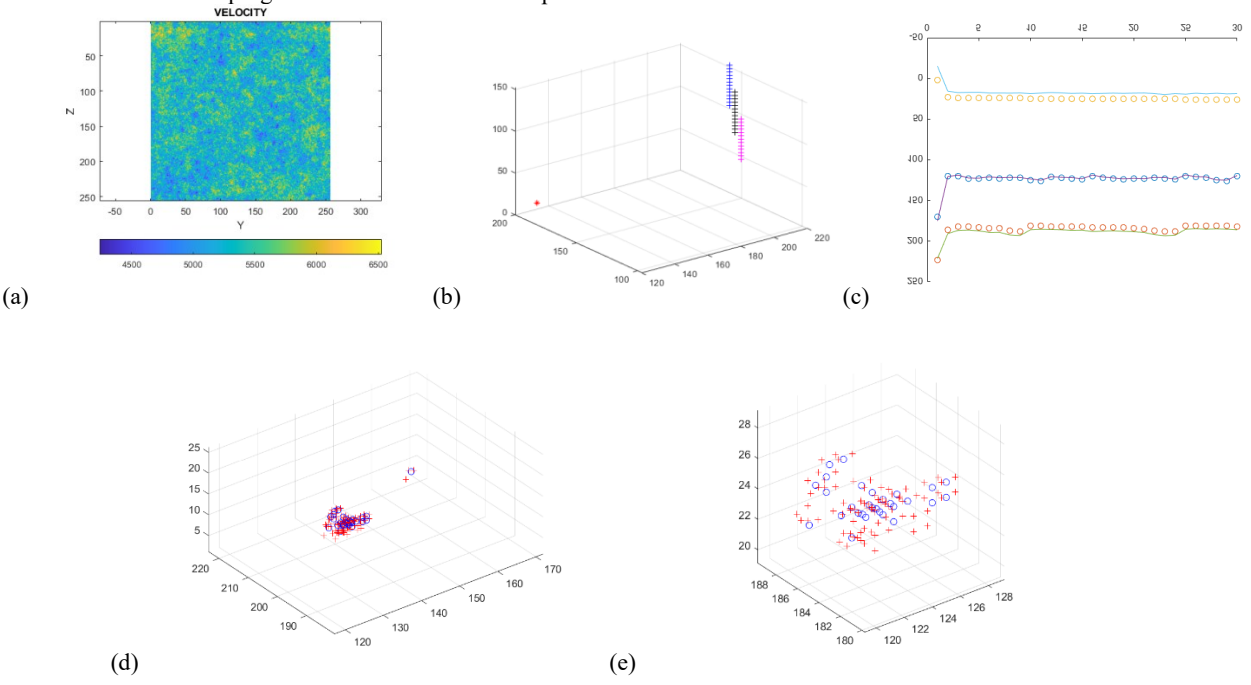

Figure 12. Numerical simulation summary of Meq surveillance of UtahForge EGS stimulation process for source-sensor geometry shown in Fig 8: (a) 2D seismic wave speed fluctuations due to pink-noise porosity distributiomn φ(x,y,z)); (b) Meq source (*) andwellbore sensors (+); (c) Nelder-Mead traveltime inversion fit (lines) to sensor travel times (o); (d) decameter-scale spatial resolution of Meq fit locations (red) to actual source locations (blue); (e) meter-scale resolutions of Meq locations.

On the basis of existing and future UtahForge observation, the Fig 1 cross-well flow structure sketch can be cast into a generic advection-conduction format in which the radial scale R of the EGS advection-conduction structure can be assessed for a given heat energy flow Q for a given crustal heat reservoir temperature lifetime τ. We can thus determine if the (existing) EGS flow stimulation process can provide a sufficiently large stimulation volume radius R for a given heat production rate Q for a given duration τ. With Fig 7 prospectively calibrating the present UtahForge EGS cross-well flow system at R ~ 50m able to produce viable heat for 3-10 years at heat production rate Q ~ 20MW, we are in a position to make systematic Meq observations to validate or adjust the Fig 7 process. With a firm Meq-based calibration of the present UtahForge EGS cross-well stimulation volume, we can, for instance, confidently assess what increase of well-to-well offset is needed to increase Q to, say, 40MW while avoiding badly depleting the heat reservoir over, say, a 20 year period.

5. DISCUSSION

In light of the foregoing deconstruction of the UtahForge EGS flow stimulation at 2.5km depth in hot crystalline rock, it is perhaps the time to openly recognise that EGS fluid interaction with the fractured ambient crust needs a science foundation outwith the engineering practices developed for hydrocarbon recovery. Canonical EGS schemes have focused on fracture flow derived from visual inspection of rock outcrops and mine free-surface exposures, e.g., [2-3] having a pipe-flow aspect expressed by the cubic-law Poiseuille flow assumption, e.g., [4-5]. Neither of these EGS tenets has any basis in the reality of crustal rock-fluid interactions attested by well-log, well-core, or well-flow data, e.g., [6-10]. The two-fold importance of the UtahForge EGS stimulation flow data is, first, the explicit failure of well-to-well hydrofracks to create well-to-well planar cubic-law flow paths as per the EGS canon, and, second, the success of the 400m-interval open wellbore pressurisation to flow at 30L/s for 30 days, with well-to-well flow beginning at small initial injector well pressures as seen in Fig 2. Also important is the return of deep-sensor Meq waveform data which clearly demonstrate that the Meq slip events do not occur on “fault-like” plane surfaces, but instead are consistent with bidirectional fluid expulsion from over-pressured permeability structures [17]. Together the UtahForge EGS flow stimulation data collectively provide direct evidence for two updated perspectives on EGS. First, ambient crust flow heterogeneity at all scales from cm to km as expressed by the poro-permeability empiric. $\kappa(x,y,z) \sim \exp(\alpha\varphi(x,y,z))$ poses serious problems for upscaling to commercial grade crustal heat extraction facilities. Second, the intimate relation between Meqs generated by EGS flid preservation with the ambient crust poro-permeability $\kappa(x,y,z) \sim \exp(\alpha\varphi(x,y,z))$ distribution provides powerful observational means by which to validate, survey, and monitor the present and future EGS stimulation projects.

REFERENCES

[1] Utah FORGE: Wells 16A(78)-32 and 16B(78)-32 Stimulation Program Report - May 2024 **DOI10.15121/2483880**
[2] Gringarten, A. C., P. A. Witherspoon, et al. (1975) Theory of Heat Extraction from Fractured Hot Dry Rock. Journal of Geophysical Research 80(8): 1120-1124.
[3] Tester JW *et al.* (2006) *The Future of Geothermal Energy -- Impact of Enhanced Geothermal Systems (EGS) on the United States in the 21st Century*, Massachusetts Institute of Technology.
[4] Sutter D, Fox DB, Anderson BJ, Koch DL, von Rohr PR &Tester JW (2011) Sustainable heat farming of geothermal systems: a case study of heat extraction and thermal recovery in a model egs fractured reservoir. *35th Workshop on Geothermal Reservoir Engineering*, Stanford University, January 31-February 2.
[5] Zhang Q and Taleghani AD (2024) Downhole flow management to enhance efficiency of fractured geothermal systems in horizontal wells, 49th Workshop on Geothermal Reservoir Engineering, Stanford University, February 12-14, SGP-TR-227 1
[6] Leary PC (2002) Fractures and physical heterogeneity in crustal rock, in *Heterogeneity of the Crust and Upper Mantle – Nature, Scaling and Seismic Properties,* J. A. Goff, & K. Holliger (eds.), Kluwer Academic/Plenum Publishers, New York, 155-186.
[7[Leary PC & Al-Kindy F (2002) Power-law scaling of spatially correlated porosity and log(permeability) sequences from north-central North Sea Brae oilfield well core, *Geophysics Journal International* 148, 426–442.
[8] Leary PC, Malin PE & Pogacnik JA (2012) Computational EGS -- heat transport in 1/f-noise fractured media**,** 37th Workshop on Geothermal Reservoir Engineering .Stanford, California, January 30 - February 1, 2012 SGP-TR-194
[9] Leary P, Malin P, Saarno T and Kukkonen (2018) $\alpha\varphi \sim \alpha\varphi crit$ – Basement rock EGS as extension of reservoir rock flow processes, 43rd Workshop on Geothermal Reservoir Engineering, Stanford University, February 12-14, SGP-TR-213 1
[10] Leary P. Malim P, Saarno T, Heikkinen P and Diningrat W (2019) Coupling crustal seismicity to crustal permeability – Power-law spatial correlation for EGS-induced and hydrothermal seismicity **,** 44th Workshop on Geothermal Reservoir Engineering, Stanford University, February 11-13, 2019 SGP-TR-214 1
[11] Simmons SF & Barker B (2025) Utah FORGE geothermal resource assessment based on stored heat. Unpublished Utah FORGE report, https://gdr.openei.org/submissions/1745.
[12] Success of Geothermal Wells: A global study (2013) International Finance Corporation -- 7230
https://ope nknowledge.worldbank.org/bitstreams/cdf75592-bb66-5feb-b138-38f7221d2366
[13] Leary P, Malin P & Niemi R (2017) Fluid flow & heat transport computation for power-law scaling poroperm media, *Geofluids*, Volume 2017, https://doi.org/10.1155/2017/9687325

[14] Leary P, Malin P, Saarno T & Kukkonen I (2017) Prospects for Assessing Enhanced Geothermal System (EGS) Basement Rock Flow Stimulation by Wellbore Temperature Data*, Energies*, vol 10 , no. 12, DOI: 10.3390/en1012197
[15] Carslaw HS & Jaeger J (1959) Conduction of Heat in Solids, Oxford University Press
[16] Rutledge J, Pankow K, Niemz P, Dyer B and Karvounis d (2025) Microseismic source mechanisms during a Utah FORGE injection stimulation, 50th Workshop on Geothermal Reservoir Engineering Stanford University, February 10-12, 2025 SGP-TR-229 1
[17] Malin PW and Leary PC (2023) Haskell Waveform Modeling of EGS Stimulation Meqs as Slow Ruptures Within Ambient Crust Permeability Structures, 48th Workshop on Geothermal Reservoir Engineering , February 6-8, 2023 SGP-TR-2243
[18] Schubert F (2012) Basic Principles of acoustic emission tomography, Journal of Acoustic Emission. https://www.ndt.net
[19] Shapiro SA, Rentsch S, and Rothert R (2003) Characterization of hydraulic properties of rocks using probability of fluid-induced micro-earthquakes, https://www.wit.uni-hamburg.de › wit2003-rentsch